Desalination and Water Treatment
www.deswater.com

doi: 10.5004/dwt.2023.29372

289 (2023) 98–110
March

Analysis of the effect of microscopic bubble collapse on the decomposition of Cr-EDTA heavy metal complexes

Yuanyuan Zhao[a], Guohui Li[b], Wei Xu[c], Rongsheng Zhu[c], Qiang Fu[c], Xiuli Wang[c,*]

[a]*School of the Environment and Safety Engineering, Jiangsu University, Zhenjiang 212013, China, email: Zyy-michelle@163.com*
[b]*GongQing Institute of Science and Technology, Gongqingcheng Shi, Jiangxi 332020, China, email: lghgqkj@163.com*
[c]*Research Center of Fluid Machinery Engineering and Technology, Jiangsu University, Zhenjiang 212013, China, emails: ujslthb@163.com (X.L. Wang), Xuwei791837@hotmail.com (W. Xu), zrs@ujs.edu.cn (R.S. Zhu), ujsfq@sina.com (Q. Fu)*

Received 8 August 2022; Accepted 20 February 2023

ABSTRACT

Industrial organic wastewater contains heavy metal ions, which are toxic, difficult to degrade, and easily accumulates in the environment. Moreover, these ions easily form a high-steady-state structure with organic complexes, thus increasing the difficulty of degradation. The mechanical and chemical effects caused by bubble collapse can effectively decompose heavy metal complexes, but its specific influence law remains unclear. This study aims to determine the relationship between the factors affecting the collapse of free state bubble and the decomplexing effect of heavy metal complexes by establishing various complex models and considering the local density of each atom in the complex as the research object. The radial distribution function of atoms was used to characterize the changes in the structure of heavy metal complexes, and the effects of bubble radius (R), compressive strain (ε), and temperature (T) on the decomplexing of heavy metal complexes were compared and analyzed. The results show that compressive strain and temperature have obvious effects in the initial stage of bubble collapse. At the same bubble radius, the compressive strain has the greatest influence on the effect of decomplexation, followed by the temperature influence. At 2,000 fs, the number of carbon atoms around the carbon atoms decreased by 40%. When the compressive strain is 0.001, the bubble radius is 20 Å, and the temperature is 308 K, the effect of decomplexation is the best. With the increase in compressive strain, the bubble radius and temperature enhanced the acceleration of the collapse of the bubble and energy release for decomplexation treatment. The theory can provide technical guidance for engineering applications and is of great significance for accelerating the progress of sewage treatment technology.

Keywords: Cavitation bubble collapses; Bubble radius; Compressive strain; Temperature; Radial distribution function

1. Introduction

The development of industry has provided an important guarantee for the improvement of social productivity and has increased the types and quantities of industrial wastewater [1]. Industrial wastewater containing heavy metal ions accounts for a large proportion of wastewater. Generally, heavy metals mainly refer to toxic lead, cadmium, chromium, mercury, and metalloid arsenic. At present, heavy metal ions are mainly derived from organic industrial wastewater from mining, printing and dyeing, papermaking, electroplating, electrolysis, and paint industries. Considering that heavy metals are difficult to degrade, toxic, and easily accumulate in the environment [2,3], and if organic industrial wastewater containing heavy metal ions is directly discharged into nearby rivers without treatment or improper treatment, the ecological environment will be damaged, thus affecting the use value of water resources and the drinking water safety

* Corresponding author.

Simulation domain size: 74 Å × 60 Å × 60 Å	Operating temperature: 288, 298, and 308 K
Cut-off radius: 9.5 Å	Thickness of the ethylenediaminetetraacetic acid wall: 5 Å
Compression strain rate: 0.0001, 0.0005, 0.001	Thickness of the Cr: 2 Å
Time step in relaxation: 1 fs	Time step in simulation: 0.25 fs
Mass of the C atom: 12.01 (dimensionless)	
Mass of the H atom: 1.008 (dimensionless)	
Mass of the O atom: 15.9994 (dimensionless)	
Mass of the N atom: 14.0067 (dimensionless)	
The radii of the cavitation: 10, 12, 15, and 20 Å	
Velocity of atoms: generated according to the Maxwell distribution under corresponding temperature	
Distance between the cavitation and the lower wall of the ethylenediaminetetraacetic acid: 10 Å	

of urban residents and restricting social and economic development.

In recent years, scholars have conducted systematic research on the degradation methods of heavy metal industrial wastewater, including physical adsorption [4–6], chemical [7], biological [8,9], and ion exchange methods [10]. In terms of physical methods, Karimi et al. [11] used adsorption to remove organic pollutants and heavy metal ions, established a mathematical model to predict the adsorption mechanism, and found that the adsorbent for removing organic pollutants and heavy metal ions in industrial wastewater was selective [12]. In terms of chemical methods, Di et al. [13] used various catalysts to catalyze the reduction of pharmaceutical pollutants and heavy metals in water. Although pentavalent and trivalent arsenic were removed together with ibuprofen, the processing cost was very high, the processing difficulty was relatively large, and secondary pollution might be introduced, and this situation is very unfavorable for cost control. Feng et al. [14] found that electrochemical treatment methods could be combined with ion exchange methods to achieve the effective removal of mixed pollutants of organic matter and heavy metals. Even at a low current density, it could be completely removed within 4 min, but the control of the device involved is complicated [15]. In terms of biological method research, Ahmad et al. [16] found that the use of bacteria and other microorganisms to deal with heavy metal pollutants is effective. Although the method has certain economic feasibility and avoids the risk of introducing secondary pollution, it is selectivity for the degradation of pollutants and has high requirements on the composition of pollutants. The above methods involve direct treatment of heavy metal ions in industrial wastewater, and the treatment process encounters problems such as long cycle, low efficiency, and secondary pollution. Heavy metal ions in organic wastewater are difficult to degrade, because they easily form complex with organic compounds, making heavy metal ions encapsulated and forming a stable state. The use of hydrodynamic cavitation technology to digest heavy metal complexes is a current research hotspot [17–20]. The technology mainly uses extreme conditions such as high temperature, high pressure, strong shock wave, and high-speed micro-jets generated by bubble collapse for the decomplexation of heavy metal complexes. The mild reaction conditions, low energy consumption, and absence of secondary pollution in the treatment process of this technology result in its broad application prospects.

The above analysis shows that dealing with the pollution of heavy metal complexes involves the removal of organic complexes on the surface, and advanced technology can deal with free heavy metal ions. At present, in the field of wastewater degradation, the use of bubble collapses to degrade organic pollutants has aroused widespread academic interest among scholars. The current research mainly focused on two aspects. First, the study focused on operating variables, and scholars had found that structural parameters of the cavitation device, initial concentration of pollutants [21], solution pH [22,23], operating pressure, solution temperature [24], and running time [25] have important effects on the degradation of organic pollutants by hydrodynamic cavitation. Second, the study focused on the synergistic degradation of pollutants by hydrodynamic cavitation and other technologies. Specifically, it referred to the combined use of hydrodynamic cavitation and chemical agents [26,27], the combined use of hydrodynamic cavitation and catalysts [23,28], and the use of hydrodynamic cavitation in combination with three or more mixed processes of chemical agents, catalysts, coagulants, and acoustic cavitation to degrade different types of pollutants [29–31]. Results showed that the degradation efficiency was improved, indicating that these technologies could degrade different pollutants, and the degradation was universal. However, the above research was conducted through macroscopic experiments. The results are insufficient to determine the quality of the process with the test results as the goal. Moreover, the mechanism of cavitation degradation cannot be accurately determined. Thus, the stability and efficiency of the degradation of pollutants in wastewater could not be effectively improved. With the development of computer technology, scholars had gradually shifted their attention to the field of microcosmic, tried to observe the dynamic process of the interaction between bubble collapse and the pollutant wall at the nanometer scale, and explored the relationship between the factors affecting the collapse of the bubble and the degradation of pollutants to determine the theory of cavitation degradation. Santo and Berkowitz [32] studied the perforation of the lipid bilayer caused by nanobubbles of different sizes exposed to shock waves of different speeds and summarized the formation of pores and the damage of the bilayer. Man et al. [33] used ultrasound to induce the shock wave released by bubble collapse to penetrate the cell membrane and form small holes in the membrane to evaluate the wall shear stress caused by bubble vibration and the mechanism of membrane pores

and explore the stable vibration molecular mechanism. Gu et al. [34] and Jackson et al. [35] used molecular dynamics simulation methods to establish two systems of nano-polyethylene particles and silica particles and studied the effect of nanoparticles on the initiation of cavitation, but they did not study the collapse of bubbles. Zhou et al. [36] studied the collapse of bubbles caused by shock waves to produce high-speed micro-jets and shock waves and found that large shear stress triggers the shedding of molybdenum disulfide, and the shock wave reflected from the surface of molybdenum disulfide enhances the spalling. Fu et al. [37] studied the collapse of bubbles of different diameters by using atomic and coarse-particle molecular dynamics simulations to calculate the force acting on the membrane, revealing the relationship between impulse and bubble radius. Adhikari et al. [38] established two systems with and without bubbles and studied the mechanism of shock wave-induced nanobubbles to rupture to form membrane pores. Nan et al. [39] established a bubble model located near the cell membrane and found that the final shape of the bubble collapse has a ring structure, and the maximum volume of the cavitation area is related to the initial bubble size.

In summary, the microscopic studies have been conducted on the use of the energy released by bubble collapse to achieve the degradation of pollutants, and the application in medicine is high. The research in this direction can provide a reference basis for the field of wastewater treatment. Researchers have mainly studied the collapse characteristics of bubbles by considering temperature, viscosity, surface tension, cavitation nucleus, and second phase particle size. A few systematic studies have focused on the influence of factor parameters, such as temperature, compressive strain, and bubble radius on bubble collapse. When the system temperature changes, its viscosity, surface tension, and saturated vapor pressure will all change, thus directly affecting the difficulty of bubble collapse. The bubble collapses when the pressure increases instantaneously, and the pressure change of the system can be characterized by the compressive strain. In this paper, compressive strain is set as the boundary condition by means of C language. The radius of the bubble determines whether the bubble can exist stably and has a great influence on the collapse of the bubble. The energy released by bubble collapse can degrade pollutants. Therefore, the system temperature, compressive strain, and bubble radius are important factors affecting the degradation of pollutants.

The paper creatively uses the extreme conditions generated by bubble collapse to decomplex heavy metal complexes. The conversion of difficult-to-handle, difficult-to-biochemical, and high-steady-state heavy metal complexes into heavy metal ions creates a prerequisite for the subsequent processing of heavy metals. The main goal is that the mechanical and chemical effects caused by bubble collapse can effectively decompose heavy metal complexes, and the paper makes the specific influence law be clear. The specific goal is that the paper aims to determine the relationship between the factors of bubble radius, compressive strain, and temperature affecting the collapse of free state bubble and the decomplexing effect of heavy metal complexes by establishing various complex models. The selected research object is the heavy metal complex formed by ethylenediaminetetraacetic acid (EDTA) and chromium, and this complex has a stable structure and hinders the harmless treatment of chromium in wastewater. The choice of the appropriate force field parameters and the development of water molecular models and EDTA molecular models close to real conditions remain a challenge. The paper is based on molecular dynamics simulation to study the changes in the radial distribution function (RDF) of atoms in the complex molecule during the bubble collapse of the free state bubble to reflect the molecular microstructure and aggregation distribution characteristics, determine the relationship between bubble radius, compressive strain, temperature, and pollutant degradation, and provide theoretical guidance for the engineering application of heavy metal processing technology.

2. Models and research methods

2.1. Force field and water molecule model selection

The calculation of classical mechanics needs to be based on the force field, and the completeness of the force field determines the accuracy of the calculation. ReaxFF [40] is a reactive force field, and it uses the principle of bond to simulate the chemical and physical interaction of atoms and molecules in a complex reaction system. Therefore, ReaxFF can provide detailed information on the formation and rupture of bonds in complex reaction systems, and the chemical reaction energy and energy barrier can be accurately calculated. Classical molecular dynamics can simulate larger systems but cannot accurately describe chemical reactions. Molecular dynamics based on reaction force field combines the advantages of quantum mechanics and classical molecular dynamics, and ReaxFF reaction force field was selected for simulation calculation. Generally, ReaxFF describes all energy items related to bond formation and breakage in the potential based on the bond level, including bond length, bond angle, torsion dihedral angle, over- and under-coordination correction, hydrogen bonding interaction and other interactions, and correction of effects such as lone pair electron energy, three-body co-rolling, and four-body conjugate. The modified Morse potential based on Taper correction was used to describe the van der Waals non-bonding interaction. The atomic point charge was used to describe the Coulomb electrostatic interaction, and the electronegativity balance theory was used to dynamically update the atomic charge at each time step.

A suitable water molecule model has an important influence on the accuracy of the simulation results. Wang et al. [41] optimized the parameters of the original four-point model TIP4P through the force balance method and proposed the TIP4P-FB model. The density, thermal expansion coefficient, isothermal compressibility, dielectric constant, autocorrelation coefficient, shear viscosity, surface tension, and maximum theoretical density of the model was studied, and the results show that they are close to the properties of actual water. The paper selected the TIP4P-FB model for molecular dynamics simulation.

2.2. Model building

According to the molecular structure information of EDTA, MS software was used to generate the initial model

of EDTA molecule, as shown in Fig. 1. EDTA consists of C, H, O, and N with a total of 36 atoms. Then, the Packmol program was used to construct the initial position of the water molecule [42], water molecules [43] and cavities are distributed in the computational domain of a cube with a side length of 60 Å, and the X, Y and Z directions are set as periodic boundary conditions. The programming language was used to add the upper and lower layers of the complex with a thickness of 5 Å in the z direction of the system, and the wall of the complex was composed of EDTA molecules. Finally, the heavy metal chromium wall was constructed on the outer side of the upper and lower complex walls to form a heavy metal complex system, as shown in Fig. 2. In the heavy metal complex system constructed by this simulation process, the radii of the cavity were 10, 12, 15, and 20 Å, and the distance between the cavity and the lower wall of the EDTA was 10 Å. In the model, the pH of the model is assumed to be neutral (pH = 7), and Cr ion is assumed to form a stable heavy metal complex system with the complex EDTA.

2.3. Boundary condition

In the simulation, the chemical reaction between the wall and the water molecule system was not considered. The cut-off radius (R_{cut}) was set to 9.5 Å, and the force field can be ignored when the interparticle distance exceeds the cutoff radius. The bond length and bond angle of TIP4P-FB water molecules were fixed using the SHAKE algorithm. During relaxation, the initialization speed of the system satisfies the Maxwell–Boltzmann distribution and is randomly generated according to the Maxwell distribution at the corresponding temperature. The Newtonian integral equation of motion was solved numerically using the velocity–Verlet algorithm. Coulomb potential (long-range force calculation) uses the particle-particle-particle-mesh method. The system uses a thermal bath coupling method to control the temperature. The actual temperature change rate is related to the temperature of the hot bath as expressed below.

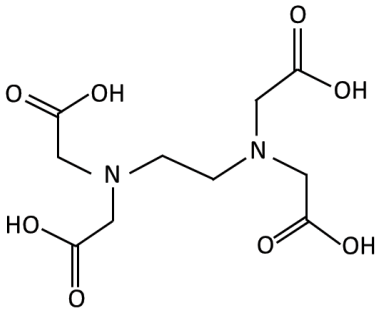

Fig. 1. Ethylenediaminetetraacetic acid structure diagram.

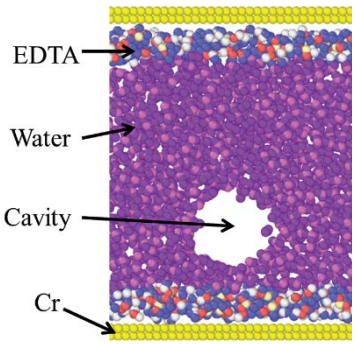

Fig. 2. Section of heavy metal complex model.

$$\frac{dT_A}{dt} = \frac{T_D - T_A}{\tau} \tag{1}$$

where T_D is thermal bath temperature, T_A is the actual temperature, and τ is the degree of coupling between the thermal bath and the system, that is the relaxation time.

Based on Eq. (1), the temperature change between successive steps can be expressed as follows:

$$\Delta T = \frac{\Delta t}{\tau}\left(T_D - T_A\right) \tag{2}$$

The corresponding speed scale is as follows:

$$\begin{cases} v_{ix}^{new} = v_{ix}\sqrt{1+\dfrac{\Delta t}{\tau}\left(\dfrac{T_D}{T_A}-1\right)} \\ v_{iy}^{new} = v_{iy}\sqrt{1+\dfrac{\Delta t}{\tau}\left(\dfrac{T_D}{T_A}-1\right)} \\ v_{iz}^{new} = v_{iz}\sqrt{1+\dfrac{\Delta t}{\tau}\left(\dfrac{T_D}{T_A}-1\right)} \end{cases} \tag{3}$$

According to Eq. (3), the trajectory of the atom can be obtained, and the collapse process of the bubble can also be analyzed.

2.4. Research methods

When performing MD calculations are performed, the entire model should be relaxed. The relaxation process is essentially a dynamic process in which microscopic particles exchange energy in the system and finally reach a stable distribution. The temperature change is an essential parameter for measuring whether the system reaches a steady state for the relaxation process. The temperature fluctuates around a constant value when the computational domain is in a steady state, as shown in Fig. 3.

The bubble collapse would release a large amount of energy and produce mechanical, chemical, and thermal effects on the heavy metal complexes in the liquid. No matter what kind of effect was acted on the complex in the ReaxFF reaction field, it could be shown through this field. Finally, the RDF was used to characterize the degradation degree of pollutants, so as to reflect the effect of cavitation without exploring the specific effect in the process of the bubble collapse. The RDF is a statistical function used to describe how the density of the system particles changes with the distance between the reference particles. During the collapse of the bubble, the $G(r)$ between atoms in the EDTA

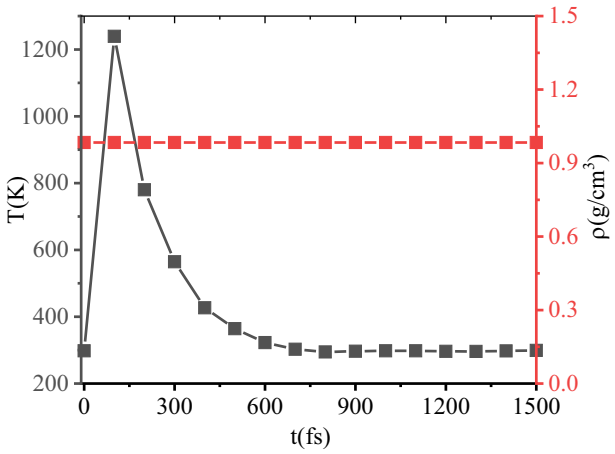

Fig. 3. Relationship between temperature, density and time during the relaxation process.

molecule can reflect the microstructure and aggregation distribution characteristics. It is defined as the ratio of the local area density at a distance r around the reference particle to the average density of the system.

When performing molecular dynamics calculations, the entire complex system was first be relaxed with bubble radii of 10, 12, 15, and 20 Å. The system adopted the canonical ensemble, and the time step is set to 1 fs. After running for 3,000 steps, the system reached the set temperature value and gradually stabilized. After the relaxation, the temperature values were 288, 298, and 308 K, and the compressive strains were 0.0001, 0.0005, and 0.001 to run the entire system with 30,000 steps with a time step of 0.25 fs. The data parameters of all molecules in the simulation area were obtained every 500 or 50 steps. Finally, the obtained data were analyzed and summarized.

3. Results and discussion

Considering that many factors affect the effect of bubble collapse and degradation of pollutants, a coupling relationship exists between the factors. The paper expounds the previous research methods and analyzes the relationship among the bubble radius, compressive strain, and temperature and the characterization of pollutant degradation. By studying the changes in the RDF of atoms in the complex molecule during the bubble collapse process, the molecular microstructure and aggregation distribution characteristics and the influence of various factors on the decomplexation of heavy metal complex pollutants were determined.

3.1. Analysis of the effect of bubble radius on the RDF of atoms in complex molecules

When the cavity of each radius collapsed at a temperature of 298 K and compressive strain of 0.0001, the RDF between the carbon–carbon atoms in EDTA molecule changed with time, as shown in Fig. 4. According to the peak values of each curve in Fig. 4, a new graph was made, as shown in Fig. 5.

Fig. 4 shows the RDF of carbon–carbon atoms in EDTA when the bubble did not collapse (t = 0 fs) and the bubble collapsed (t = 500, 1,000, 2,000, and 4,000 fs). When r < 1.4 Å, the value of $G(r)$ is approximately 0, indicating that the nearest distance between carbon and carbon in the EDTA molecule is 0.14 nm. When r is between 1.4 and 5.8 Å, the value of $G(r)$ fluctuates, indicating that the local area density of carbon atoms is quite different from the average density of the system. When r > 5.8 Å, the value of $G(r)$ gradually tends to be unchanged. An obvious peak was observed on the whole curve, and the peak quickly declined as the distance increased until it became stable. Results show that the energy released by the collapse of the bubble acts on the carbon atoms, and it reduced the value of the RDF of the carbon atoms, decreased the local area density of carbon atoms, and decreased the number of carbon atoms around carbon atoms. The carbon–carbon bonds were broken, and the molecular structure of EDTA changed, thus playing a role in degradation.

As shown in Figs. 4 and 5, when r = 1.6 Å, based on the comparison of the $G(r)$ peaks of different bubble radii, as the radius of the cavity increased, the peak value of $G(r)$ slightly changed at 0 fs. Therefore, when bubble collapse does not occur, the distribution of atoms around the carbon is consistent. With the increase of the bubble radius, the peak value of $G(r)$ first increased and then decreased. As shown in Fig. 5, the peak value of $G(r)$ decreased significantly at the beginning with the increase of the bubble radius, indicating that large-radius bubbles are obvious to the initial stage of degradation. Under the same bubble radius, as time changed, the peak value of the $G(r)$ gradually decreased, indicating that the local density of carbon atoms in EDTA decreased, and the number of carbon atoms around the carbon atoms decreased. At 2,000 fs, the peak value of $G(r)$ remarkably decreased, and the number of carbon atoms around the carbon atoms decreased by approximately 40%. This phenomenon may have occurred because the bubbles of each radius released the maximum pressure to form a huge shock wave, resulting in impact shearing effect on the surface of the complex and causing the carbon–carbon bond in EDTA to break.

As shown in Fig. 6, under the same bubble radius, with the change of time, the peak value of the $G(r)$ gradually decreased, indicating that the local density of nitrogen atoms in EDTA decreased. The $G(r)$ peak value quickly decreased at 500 fs, and this phenomenon may be related to the molecular structure of EDTA. Moreover, the nitrogen atoms in the molecule are not directly connected by valence bonds. When the pressure released by the collapse of the bubble acts on the EDTA molecule, the non-valent bond between nitrogen and nitrogen may result in deflection, and extrusion may not occur, and making it easier to be destroyed. Hence, the $G(r)$ peak was remarkably reduced at 500 fs. At 2,000 fs, the number of nitrogen atoms around the nitrogen atom was reduced by approximately 30%. This phenomenon may be attributed to the bubbles of each radius that released the maximum pressure to form a huge shock wave, resulting in an impact shearing effect on the surface of the complex and subsequent EDTA molecular structure change.

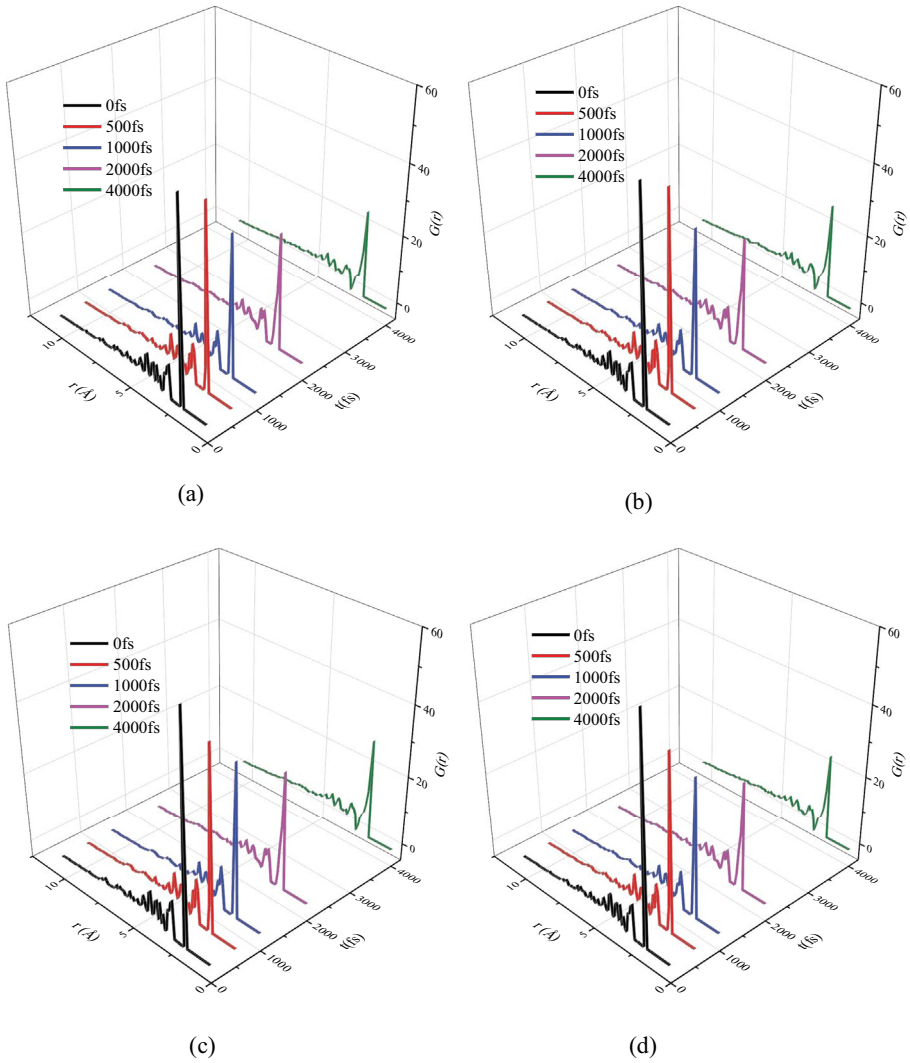

Fig. 4. Radial distribution function of carbon–carbon atoms in ethylenediaminetetraacetic acid with different bubble radii.

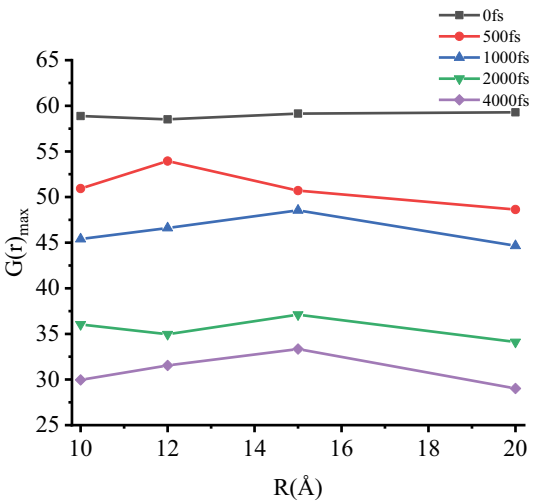

Fig. 5. Graph of the change of the peak value of carbon–carbon $G(r)$ with the bubble radius at different times.

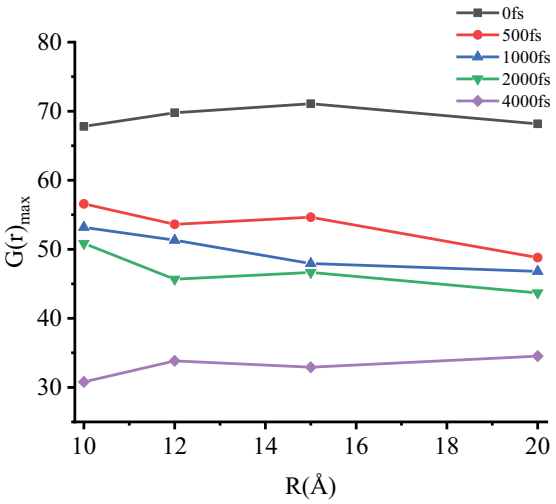

Fig. 6. Change of the peak value of nitrogen atom $G(r)$ with the bubble radius at different times.

3.2. Analysis of the effect of compressive strain on the RDF of atoms in complex molecules

To accurately determine the effect of compressive strain on the decomplexation of heavy metal complex pollutants, we have studied the $G(r)_{max}$ between carbon–carbon atoms in the EDTA molecule by the collapse of the bubbles of each radius at 298 K with compressive strains of 0.0001, 0.0005, and 0.001. Moreover, we compared the size of $G(r)_{max}$ to reflect the characteristics of the atomic microstructure and aggregation distribution at this moment. Considering the absence of chemical bond between the nitrogen–nitrogen atoms in the EDTA molecule, only the RDF $G(r)_{max}$ between nitrogen and nitrogen atoms in the EDTA molecule was studied at compressive strains of 0.0005 and 0.001.

The lines in Fig. 7 indicate that when the bubbles of different radii collapsed under different compressive strains, the maximum RDF between the carbon–carbon atoms in EDTA changes with time. Fig. 7a shows that the maximum RDF between the carbon–carbon atoms in EDTA first increased with time, decreases slowly and then rapidly, and finally remained unchanged. Therefore, the bubble collapsed slowly, releasing energy to make the EDTA molecule be squeezed first, and the local density between carbon atoms in EDTA increased. The carbon–carbon chemical bond breaks if it cannot withstand the squeezing force, and the local density between carbon–carbon atoms in EDTA decreases. As shown in Fig. 7b, the maximum RDF between carbon–carbon atoms in EDTA decreased slowly with time, then decreased rapidly, and finally remained unchanged. As shown in Fig. 7c, the maximum RDF between carbon–carbon atoms in EDTA decreased rapidly with time, and then remained unchanged. This phenomenon indicates that the energy released by the bubble collapse reduced the local density between the carbon–carbon atoms in EDTA, the chemical bond between carbon and carbon was broken, and the $G(r)_{max}$ between carbon–carbon atoms decreased. When the energy released by the bubble collapse was transformed, the local density of carbon atoms remained unchanged. Hence, the $G(r)_{max}$ between carbon–carbon atoms remain unchanged. When the compressive strain was 0.001, the rate of decrease of $G(r)_{max}$ between carbon–carbon atoms was much greater than when the compressive strains were 0.0001 and 0.0005, indicating that cavitation releases energy quickly at large compressive strains.

The line in Fig. 8 indicates that under different compressive strains, when bubbles with different radii collapse, the maximum RDF between nitrogen–nitrogen atoms in EDTA changes with time. As shown in Fig. 8, the maximum RDF between nitrogen–nitrogen atoms in EDTA first decreases

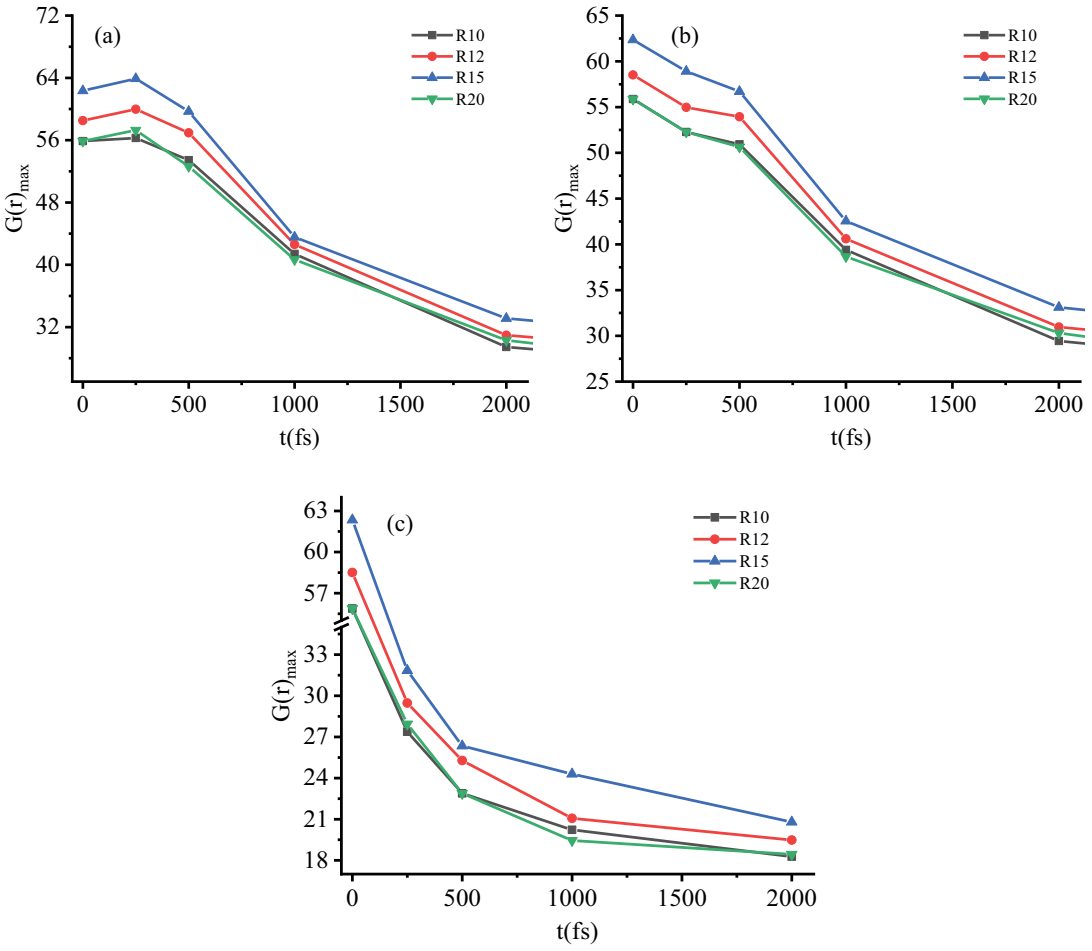

Fig. 7. $G(r)_{max}$ between carbon–carbon atoms change with time under different compressive strains.

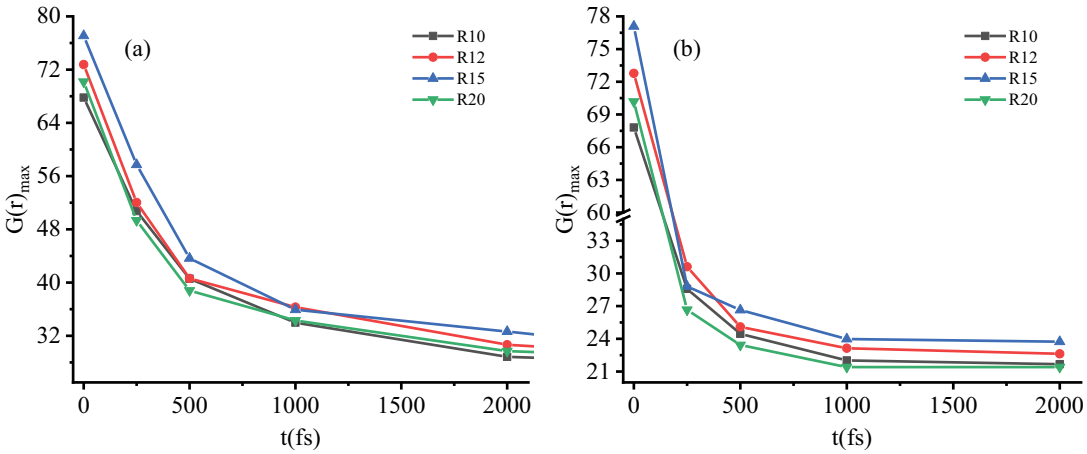

Fig. 8. $G(r)_{max}$ between nitrogen–nitrogen atoms change with time under different compressive strains.

with time, and then remains unchanged. When the compressive strain is 0.001, the rate of decrease of $G(r)_{max}$ between nitrogen–nitrogen atoms is much faster than when the compressive strain is 0.0005, and the final $G(r)_{max}$ is basically same at the two compressive strains. In the 0–1,000 fs stage, the maximum $G(r)$ value between the nitrogen–nitrogen atoms at the two compressive strain rates decreased rapidly, indicating that the energy released by the bubble was the largest during that period. The nitrogen atoms in EDTA are not connected by chemical bonds. When the nitrogen atom received the energy released by the collapse of the bubble, it can be deflected, the local density of nitrogen atoms and the $G(r)_{max}$ between nitrogen atoms decreased rapidly. As shown in Figs. 7 and 8, the large compressive strain rate affected the initial stage of bubble collapse, and the peak value of the atomic RDF decreased rapidly.

3.3. Analysis of the effect of temperature on the RDF of atoms in complex molecules

To determine the effect of temperature on the decomplexation of heavy metal complex pollutants, we studied the $G(r)_{max}$ between carbon–carbon and nitrogen–nitrogen atoms in EDTA molecule by the collapse of the bubbles of each radius at temperature values of 288, 298, and 308 K and compressive strain rate of 0.001. We also compared the size of $G(r)_{max}$ to determine the characteristics of the atomic microstructure and aggregation distribution.

The lines in Fig. 9 indicate that at different temperatures, when bubbles with different radii collapse, the maximum RDF between carbon–carbon atoms in EDTA changes with time. By comparison, the maximum RDF between carbon–carbon atoms in EDTA decreased rapidly at 250 fs. Therefore, the energy released by the bubble was the largest at 0–250 fs, and the maximum value of the RDF of carbon–carbon atoms in the complex molecule no longer changed after the energy release was over. At 288 and 298 K, the rate of decrease of $G(r)_{max}$ between carbon–carbon atoms at 250 fs is much smaller than that at 308 K, and the final $G(r)_{max}$ was basically same at the two compressive strains. Therefore, at 308 K, the bubble collapses and releases energy faster than it does at 288 K. This finding indicates that the velocity of energy released by bubble collapse increases with the increase of temperature. By studying the variation of $G(r)_{max}$ between carbon–carbon atoms with time, the influence of temperature on its collapse is more obvious when the initial volume of the bubble is small, and this phenomenon also just verify the findings of Zhang et al. [44].

The lines in Fig. 10 indicate that when the bubbles of different radii collapse at different temperatures, the maximum RDF between nitrogen–nitrogen atoms in EDTA changes with time. Moreover, Fig. 10 indicates that the maximum RDF between nitrogen–nitrogen atoms in EDTA decreases rapidly at 250 fs, and to the value tends to remain unchanged. Therefore, the energy released by the bubble is the largest within 0–250 fs, and the maximum value of the RDF of nitrogen–nitrogen atoms in the complex molecule no longer changes after the energy release is over. At 288 K, the rate of decrease of $G(r)_{max}$ between nitrogen–nitrogen atoms at 250 fs is much smaller than that at 308 K, and the final $G(r)_{max}$ is basically same at the two compressive strains. Figs. 9 and 10 show that the increase of temperature is conducive to the rapid release of energy when the bubble collapses. This phenomenon has an obvious influence on the initial stage of bubble collapse, and the peak value of the RDF of atoms decreased rapidly, but did not affect the amount of energy released.

3.4. Normalization

The paper normalizes the obtained data to compare the effects of different compressive strains and bubble radii on the $G(r)_{max}$ between carbon–carbon atoms and nitrogen–nitrogen atoms in the EDTA complex. The carbon–carbon and nitrogen–nitrogen atoms of the $G(r)_{max}$ at each compressive strain and bubble radius at 0 fs were used as refence and recorded as $G(r)_{max0}$. The normalization formula $w = [G(r)_{max} - G(r)_{max0}]/G(r)_{max0} = \Delta G(r)/G(r)$ was used to calculate the rate of change of $G(r)_{max}$ of carbon–carbon and nitrogen–nitrogen atoms at different moments for each compressive strain and bubble radius.

Figs. 11 and 12 show that when the bubble radius is large, the $G(r)_{max}$ value between nitrogen–nitrogen and carbon–carbon atoms in EDTA has a larger change, that is, the

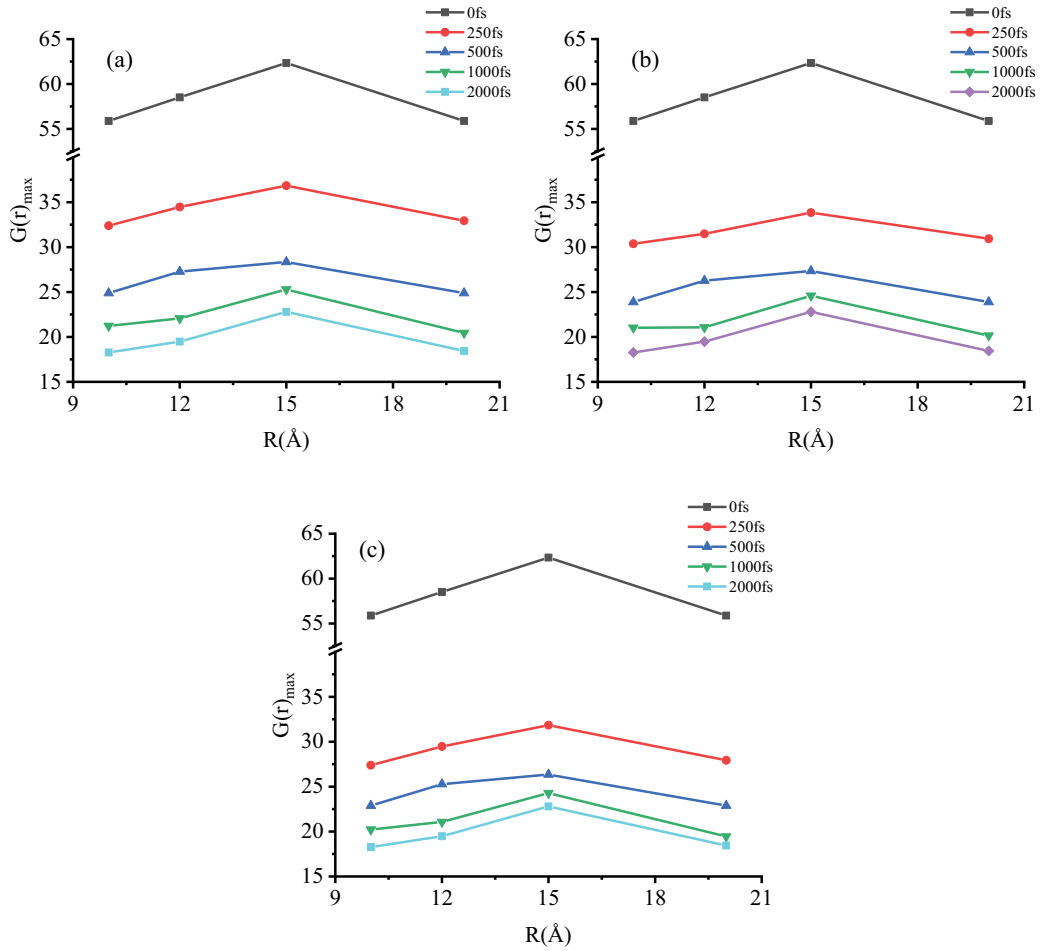

Fig. 9. $G(r)_{max}$ between carbon–carbon atoms change with time at different temperatures.

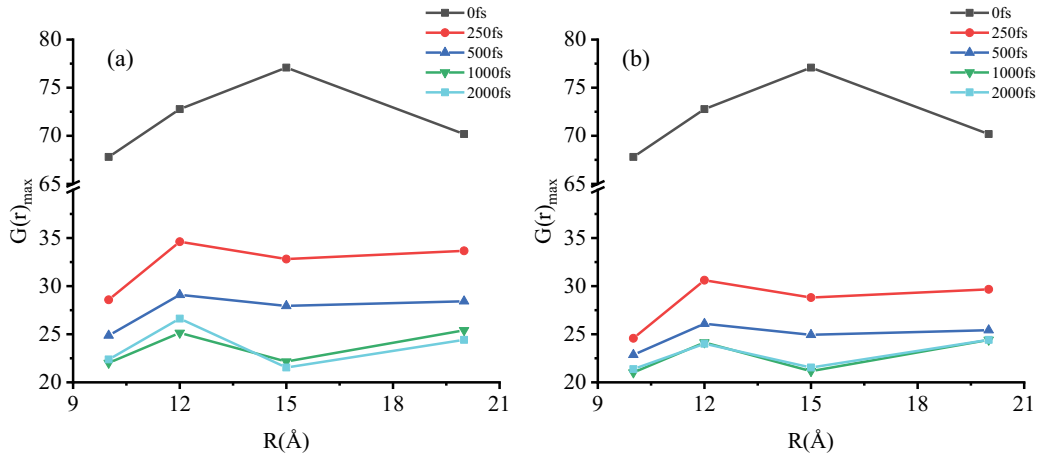

Fig. 10. $G(r)_{max}$ between nitrogen–nitrogen atoms change with time at different temperatures.

compressive strain has a more obvious effect on the bubble with a larger radius. The compressive strain has an effect on the energy release time of the bubble, and the greater the compressive strain, the faster the energy is released by the bubble. The local density between carbon–carbon atoms decreases when the local density of nitrogen atoms decreases rapidly. When the energy is fully released by the collapse of the bubble, the local density of carbon–carbon and nitrogen–nitrogen atom remains unchanged. The above figure directly indicates the relationships in Figs. 7 and 8. The chemical

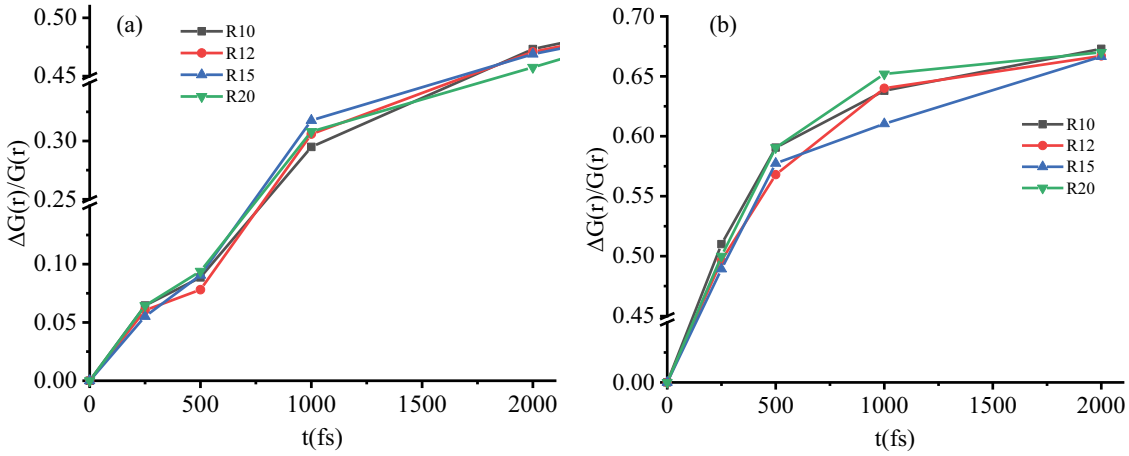

Fig. 11. Change rate of $G(r)_{max}$ between carbon atoms changes with time under different compressive strains.

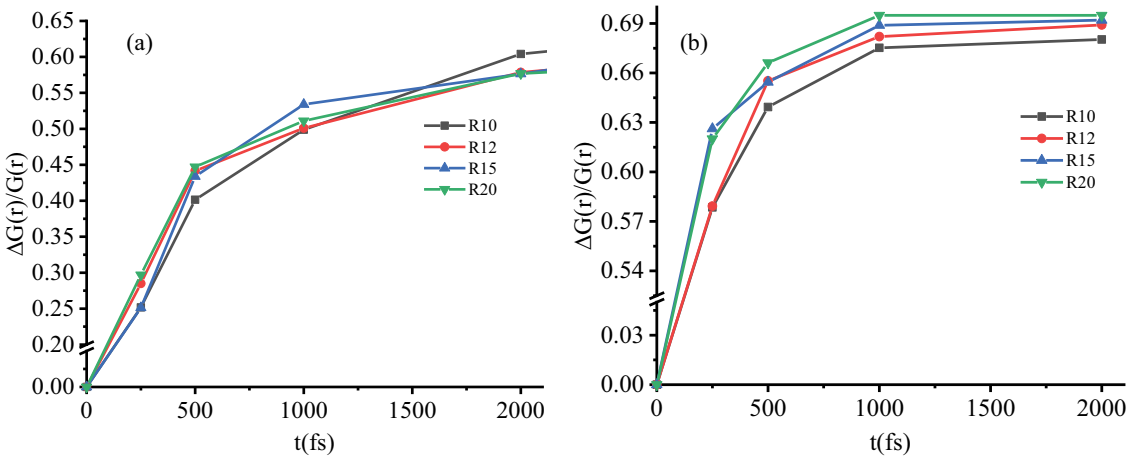

Fig. 12. Change rate of $G(r)_{max}$ between nitrogen atoms changes with time under different compressive strains.

bond between carbon and carbon in the EDTA molecule breaks upon exceeding a certain deformation. Therefore, the local density between carbon atoms decreases slowly, and then decreases rapidly, and when the energy from the bubble collapse is fully released, the local density of carbon atoms remains basically unchanged. Hence, the $G(r)_{max}$ between the carbon atoms tends to remain unchanged. The nitrogen atoms in EDTA are not connected by chemical bonds. When the nitrogen atom receives the energy released by the collapse of the bubble, it is more easily destroyed, and the local density of the nitrogen atom decreases rapidly.

To compare the influence of temperature, compressive strain, and cavity radius on the primary and secondary relationship of the decomplexation, the data of temperature and bubble radius obtained from the study were normalized. The carbon–carbon and nitrogen–nitrogen atoms of the $G(r)_{max}$ at each temperature and bubble radius at 0 fs were used as the reference and recorded as $G(r)_{max0}$. The normalization formula $w = [G(r)_{max} - G(r)_{max0}]/G(r)_{max0} = \Delta G(r)/G(r)$ was used to calculate the change rate of $G(r)_{max}$ of carbon–carbon and nitrogen–nitrogen atoms at different moments for each temperature and bubble radius.

Figs. 13 and 14 show that when the bubble collapses, the temperature has an obvious effect on the bubble with a smaller radius, and as the temperature increases, the growth rate of $G(r)_{max}$ between nitrogen–nitrogen and carbon–carbon atom increases in EDTA. Under the same bubble radius, the final value of the w between nitrogen–nitrogen and carbon–carbon atoms are the same under the action of two temperatures. Temperature affects the time for nitrogen and carbon atoms in EDTA to reach the final state, and the higher the temperature, the faster the bubble releases energy. Therefore, the local density between carbon and nitrogen atoms decreases rapidly, and when the energy from the collapse of the bubble is fully released, the local density of carbon and nitrogen atoms remains unchanged. The above figure directly shows the relationships in Figs. 9 and 10.

Figs. 11–14 show that temperature, compressive strain, and bubble radius affect the decomplexation effect of heavy metal complexes. Based on the value of the change rate of the atomic RDF(w), the analysis and comparison show that, under the same bubble radius, the compressive strain has the greatest influence, followed by temperature. The size of the bubble radius directly determines whether the

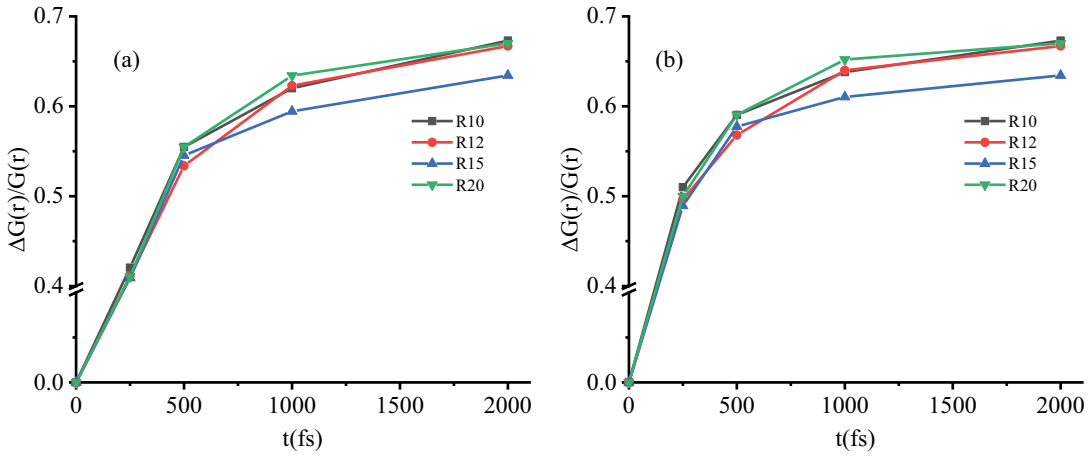

Fig. 13. Change rate of $G(r)_{max}$ between carbon atoms changes with time at different temperatures.

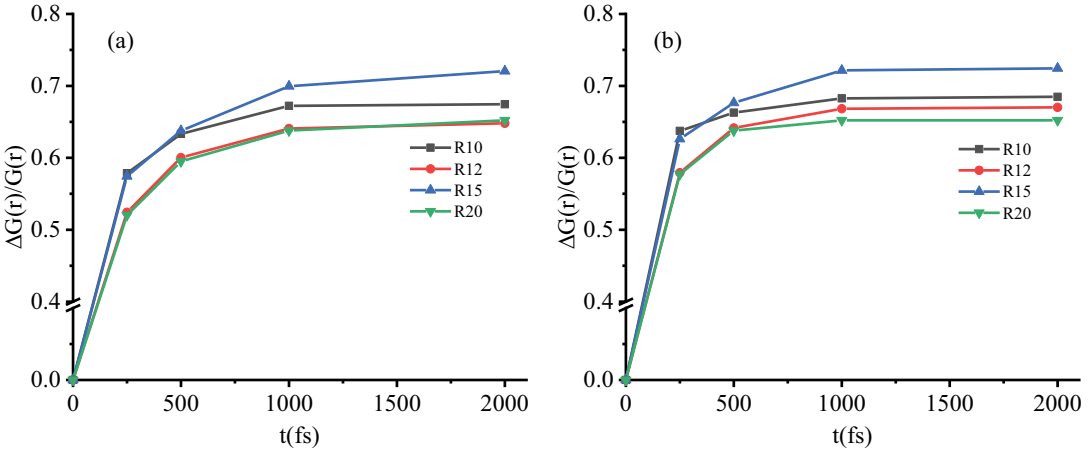

Fig. 14. Change rate of $G(r)_{max}$ between nitrogen atoms changes with time at different temperatures.

stability of the bubble. Only in this condition can we discuss the collapse of bubbles, which is key influential factor. Finally, the study found a coupling relationship between the three factors.

4. Conclusions

By establishing a complex model containing bubbles, molecular dynamics simulation methods were used to process the model, and the results show the influence of compressive strain and bubble radius on the decomplexation characteristics of heavy metal complexes when the bubble collapses, and the conclusions of the study are summarized as follows: When the compressive strain, bubble radius and temperature increases, the time for the bubble collapse is shortened. The compressive strain has a more obvious influence when the initial volume of the bubble is large. When the compressive strain is small, the maximum RDF between carbon–carbon atoms in EDTA first increases with time, and the bubble collapses slowly by releasing energy to make the local density between carbon atoms in EDTA become larger. The influence of temperature on its collapse is more obvious when the initial volume of the bubble is small. Under the same bubble radius, compressive strain has the greatest influence, followed by temperature. When the compressive strain is 0.001, the bubble radius is 20 Å, and the system temperature is 308 K, the heavy metal complex has the best effect of decomplexation.

Results that when the bubble collapses, the initial bubble radius, compressive strain, and temperature have an effect on the decomplexation of heavy metal complexes. Results show that the collapse of the bubble causes the local density of carbon and nitrogen atoms in the EDTA molecule to decrease, and they change the molecular structure and play a degrading effect. However, at present, how to accurately choose the force field, the system of the medium, and the model material and construct the gas core close to the real water is essential. In addition, the paper elaborates previous method and ignores the scale effect of water molecules, and it has certain limitations. Most of the existing studies have conducted qualitative analysis on the characteristics that affect the collapse of the bubble. Many challenges remain in the quantitative study of the influencing factors of bubble collapse. This research provides theoretical guidance

for revealing the mechanism of cavitation degradation and cavitation degradation experiments. For the study of the critical size of bubbles, the team will have a special discussion in the follow-up scientific research.

Declarations

Ethical approval and consent to participate

Not applicable

Consent for publication

Not applicable

Availability of data and materials

The datasets used and/or analyzed during the current study are available from the corresponding author on reasonable request.

Competing interests

The authors declare that they have no competing interests.

Funding

This work was supported by Key projects of the joint fund of the National Natural Science Foundation of China [U20A20292]; The Fundamental Research Funds for the Central Universities [NO: JZ2021HGB0090]; Key R&D Program of Zhenjiang City [GY2020015].

References

[1] L. Schweitzer, J. Noblet, Water Contamination and Pollution, Green Chemistry, Elsevier, Netherlands, 2018, pp. 261–290, doi: 10.1016/B978-0-12-809270-5.00011-X.
[2] K.H. Vardhan, P.S. Kumar, R.C. Panda, A review on heavy metal pollution, toxicity and remedial measures: current trends and future perspectives, J. Mol. Liq., 290 (2019) 111197, doi: 10.1016/j.molliq.2019.111197.
[3] C.C. Osuna-Martínez, M.A. Armienta, M.E. Bergés-Tiznado, F. Páez-Osuna, Arsenic in waters, soils, sediments, and biota from Mexico: an environmental review, Sci. Total Environ., 752 (2021) 142062, doi: 10.1016/j.scitotenv.2020.142062.
[4] S.D. Yang, Z.Y. Qu, W.F. Zhang, Z. Li, Y.H. Ding, Y.L. Jia, Q. Fan, Study on drip irrigation anti-clogging experiment of Yellow River water treated with inorganic adsorbent, J. Drain. Irrig. Mach. Eng., 38 (2020) 517–522.
[5] G.P. Hu, Q.H. Zhao, L.F. Tao, P.N. Xiao, P.A. Webley, K.G. Li, Enrichment of low grade CH_4 from N_2/CH_4 mixtures using vacuum swing adsorption with activated carbon, Chem. Eng. Sci., 229 (2021) 116152, doi: 10.1016/j.ces.2020.116152.
[6] M. Arshadi, M.J. Amiri, S. Mousavi, Kinetic, equilibrium and thermodynamic investigations of Ni(II), Cd(II), Cu(II) and Co(II) adsorption on barley straw ash, Water Resour. Ind., 6 (2014) 1–17.
[7] W. Xu, R.S. Zhu, J. Wang, Q. Fu, X.L. Wang, Y.Y. Zhao, G.H. Zhao, Molecular dynamics simulations of the distance between the cavitation bubble and benzamide wall impacting collapse characteristics, J. Cleaner Prod., 352 (2022) 131633, doi: 10.1016/j.jclepro.2022.131633.
[8] R.K. Sahu, R. Shankar, P. Mondal, S. Chand, Treatment potential of EC towards bio-digester effluent: effects of process parameters, aeration, and adsorbent, Desal. Water Treat., 54 (2015) 1912–1924.
[9] R. Shankar, A.K. Varma, P. Mondal, S. Chand, Treatment of biodigester effluent through EC followed by MFC: pollutants removal and energy perspective, Environ. Prog. Sustainable Energy, 38 (2019) 13139, doi: 10.1002/ep.13139.
[10] J.W. Wu, T. Wang, J.W. Wang, Y.S. Zhang, W.-P. Pan, A novel modified method for the efficient removal of Pb and Cd from wastewater by biochar: enhanced the ion exchange and precipitation capacity, Sci. Total Environ., 754 (2021) 142150, doi: 10.1016/j.scitotenv.2020.142150.
[11] S. Karimi, Y.M. Tavakkoli, R.R. Karri, A comprehensive review of the adsorption mechanisms and factors influencing the adsorption process from the perspective of bioethanol dehydration, Renewable Sustainable Energy Rev., 107 (2019) 535–553.
[12] M. Czikkely, E. Neubauer, I. Fekete, P. Ymeri, C. Fogarassy, Review of heavy metal adsorption processes by several organic matters from wastewaters, Water, 10 (2018) 1377, doi: 10.3390/w10101377.
[13] G. Di, Z. Zhu, H. Zhang, J. Zhu, H.T. Lu, W. Zhang, Y.L. Qiu, L.Y. Zhu, S. Küppers, Simultaneous removal of several pharmaceuticals and arsenic on Zn-Fe mixed metal oxides: combination of photocatalysis and adsorption, Chem. Eng. J., 328 (2017) 141–151.
[14] Y.J. Feng, L.S. Yang, J.F. Liu, B.E. Logan, Electrochemical technologies for wastewater treatment and resource reclamation, Environ. Sci. Water Res. Technol., 2 (2016) 800–831.
[15] V. Ya, N. Martin, Y.H. Chou, Y.M. Chen, K.H. Choo, S.S. Chen, C.W. Li, Electrochemical treatment for simultaneous removal of heavy metals and organics from surface finishing wastewater using sacrificial iron anode, J. Taiwan Inst. Chem. Eng., 83 (2018) 107–114.
[16] I. Ahmad, M. Imran, M.B. Hussain, S. Hussain, Chapter 7 – Remediation of Organic and Inorganic Pollutants from Soil: The Role of Plant-Bacteria Partnership, N.A. Anjum, Ed., Chemical Pollution Control with Microorganisms, Nova Publishers, New York, USA, 2017, pp. 197–243.
[17] Y.K. Lee, J.G. Han, D.C. Kim, S.K. You, G. Hong, Effect of nano-bubble on removal of complex heavy metals, J. Korean Geosynth. Soc., 14 (2015) 139–146.
[18] M. Gągol, A. Przyjazny, G. Boczkaj, Highly effective degradation of selected groups of organic compounds by cavitation based AOPs under basic pH conditions, Ultrason. Sonochem., 45 (2018) 257–266.
[19] M. Gągol, R.D.C. Soltani, A. Przyjazny, G. Boczkaj, Effective degradation of sulfide ions and organic sulfides in cavitation-based advanced oxidation processes (AOPs), Ultrason. Sonochem., 58 (2019) 104610, doi: 10.1016/j.ultsonch.2019.05.027.
[20] W. Xu, R.S. Zhu, Q. Fu, X.L. Wang, Y.Y. Zhao, G.H. Zhao, J. Wang, Analysis of the influence of factor parameters on bubble collapse in a heavy metal complex system, J. Mol. Liq., 347 (2022) 118377, doi: 10.1016/j.molliq.2021.118377.
[21] O.G. Dubrovskaya, V.A. Kulagin, L.M. Yao, The alternative method of conditioning industrial wastewater containing heavy metals based on the hydrothermodynamic cavitation technology, IOP Conf. Ser.: Mater. Sci. Eng., 941 (2020) 012009, doi: 10.1088/1757-899X/941/1/012009.
[22] I.C. Park, S.J. Kim, Effect of pH of the sulfuric acid bath on cavitation erosion behavior in natural seawater of electroless nickel plating coating, Appl. Surf. Sci., 483 (2019) 194–204.
[23] W. Xu, R.S. Zhu, Q. Fu, X.L. Wang, Y.Y. Zhao, J. Wang, Effect of bubble collapse combined with oxidants on the benzamide by molecular dynamics simulation, Ind. Eng. Chem. Res., 61 (2022) 5984–5993.
[24] S. Raut-Jadhav, D. Saini, S. Sonawane, A. Pandit, Effect of process intensifying parameters on the hydrodynamic cavitation based degradation of commercial pesticide (methomyl) in the aqueous solution, Ultrason. Sonochem., 18 (2016) 283–293.
[25] A.J. Barik, P.R. Gogate, Degradation of 4-chloro 2-aminophenol using a novel combined process based on hydrodynamic cavitation, UV photolysis and ozone, Ultrason. Sonochem., 30 (2016) 70–78.
[26] S. Saxena, V.K. Saharan, S. George, Enhanced synergistic degradation efficiency using hybrid hydrodynamic cavitation

for treatment of tannery waste effluent, J. Cleaner Prod., 198 (2018) 1406–1421.
[27] R.K. Joshi, P.R. Gogate, Degradation of dichlorvos using hydrodynamic cavitation based treatment strategies, Ultrason. Sonochem., 19 (2012) 532–539.
[28] S. Rajoriya, S. Bargole, V.K. Saharan, Degradation of a cationic dye (Rhodamine 6G) using hydrodynamic cavitation coupled with other oxidative agents: reaction mechanism and pathway, Ultrason. Sonochem., 34 (2017) 183–194.
[29] X.N. Wang, J.Q. Jia, Y.L. Wang, Combination of photocatalysis with hydrodynamic cavitation for degradation of tetracycline, Chem. Eng. J., 315 (2017) 274–282.
[30] P. Thanekar, M. Panda, P.R. Gogate, Degradation of carbamazepine using hydrodynamic cavitation combined with advanced oxidation processes, Ultrason. Sonochem., 40 (2018) 567–576.
[31] P. Thanekar, P.R. Gogate, Combined hydrodynamic cavitation based processes as an efficient treatment option for real industrial effluent, Ultrason. Sonochem., 53 (2019) 202–213.
[32] K.P. Santo, M.L. Berkowitz, Shock wave interaction with a phospholipid membrane: coarse-grained computer simulations, J. Chem. Phys., 140 (2014) 054906, doi: 10.1063/1.4862987.
[33] V.H. Man, P.M. Truong, M.S. Li, J.M. Wang, N. Van-Oanh, P. Derreumaux, P.H. Nguyen, Molecular mechanism of the cell membrane pore formation induced by bubble stable cavitation, J. Phys. Chem. B, 123 (2019) 71–78.
[34] Y.W. Gu, B.X. Li, M. Chen, An experimental study on the cavitation of water with effects of SiO_2 nanoparticles, Exp. Therm. Fluid Sci., 79 (2016) 195–201.
[35] S. Jackson, A. Nakano, P. Vashishta, R.K. Kalia, Electrostrictive cavitation in water induced by a SnO_2 nanoparticle, ACS Omega, 4 (2019) 22274–22279.
[36] G.Q. Zhou, P. Rajak, S. Susarla, P.M. Ajayan, R.K. Kalia, A. Nakano, P. Vashishta, Molecular Simulation of MoS_2 exfoliation, Sci. Rep.-UK, 8 (2018) 16761, doi: 10.1038/s41598-018-35008-z.
[37] H.H. Fu, J. Comer, W.S. Cai, C. Chipot, Sonoporation at small and large length scales: effect of cavitation bubble collapse on membranes, J. Phys. Chem. Lett., 6 (2015) 413–418.
[38] U. Adhikari, A. Goliaei, M.L. Berkowitz, Mechanism of membrane poration by shock wave induced nanobubble collapse: a molecular dynamics study, J. Phys. Chem. B, 119 (2015) 6225–6234.
[39] N. Nan, D.Q. Si, G.H. Hu, Nanoscale cavitation in perforation of cellular membrane by shock-wave induced nanobubble collapse, J. Chem. Phys., 149 (2018) 074902, doi: 10.1063/1.5037643.
[40] A.C.T.V. Duin, S. Dasgupta, F. Lorant, W.A. Goddard, ReaxFF: a reactive force field for hydrocarbons, J. Phys. Chem. A, 105 (2001) 9396–9409.
[41] L.P. Wang, T.J. Martinez, V.S. Pande, Building force fields: an automatic, systematic, and reproducible approach, J. Phys. Chem. Lett., 5 (2014) 1885–1891.
[42] L. Martínez, R. Andrade, E.G. Birgin, J.M. Martínez, PACKMOL: a package for building initial configurations for molecular dynamics simulations, J. Comput. Chem., 30 (2009) 2157–2164.
[43] J.L.F. Abascal, M.A. Gonzalez, J.L. Aragones, C. Valeriani, Homogeneous bubble nucleation in water at negative pressure: a Voronoi polyhedra analysis, J. Chem. Phys., 135 (2013) 084508, doi: 10.1063/1.4790797.
[44] Y. Zhang, A. Sam, J.A. Finch, Temperature effect on single bubble velocity profile in water and surfactant solution, Colloids Surf., A, 223 (2003) 45–54.